Spanwise spreading of gypsum slurry during deposition on the belt under a roller

Kim, Yong Il; Sanchez, Caesar; Podstawski, David; Westerweel, Jerry; Yarin, Alexander L.

DOI
10.1063/5.0276243

Publication date
2025

Document Version
Final published version

Published in
Journal of Applied Physics

Citation (APA)
Kim, Y. I., Sanchez, C., Podstawski, D., Westerweel, J., & Yarin, A. L. (2025). Spanwise spreading of gypsum slurry during deposition on the belt under a roller. *Journal of Applied Physics*, *137*(22), Article 224702. https://doi.org/10.1063/5.0276243

RESEARCH ARTICLE | JUNE 09 2025

Spanwise spreading of gypsum slurry during deposition on the belt under a roller

Yong Il Kim ; Caesar Sanchez ; David Podstawski ; Jerry Westerweel ; Alexander L. Yarin

J. Appl. Phys. 137, 224702 (2025)
https://doi.org/10.1063/5.0276243

Journal of Applied Physics ARTICLE pubs.aip.org/aip/jap

Spanwise spreading of gypsum slurry during deposition on the belt under a roller

Cite as: J. Appl. Phys. **137**, 224702 (2025); doi: 10.1063/5.0276243
Submitted: 16 April 2025 · Accepted: 19 May 2025 ·
Published Online: 9 June 2025

View Online Export Citation CrossMark

Yong Il Kim,[1] Caesar Sanchez,[1] David Podstawski,[1] Jerry Westerweel,[2] and Alexander L. Yarin[1,a)]

AFFILIATIONS

[1]Department of Mechanical and Industrial Engineering, University of Illinois at Chicago, 842 W. Taylor St., Chicago, Illinois 60607-7022, USA
[2]Laboratory for Aero and Hydrodynamics, Delft University of Technology, Mekelweg 2, 2628 CD Delft, The Netherlands

[a)]**Author to whom correspondence should be addressed:** ayarin@uic.edu

ABSTRACT

An experimental setup was designed and built to explore the spreading of a slurry layer during deposition on a moving belt before a rotating roller. The case of the water-to-stucco ratio of 75 was studied. The roller could be at rest (no rotation) or in co-rotation and counter-rotation compared to the directional motion of the spreading plastic belt (parchment paper). The widening of the slurry layer was measured and compared with the predictions of the theory developed previously by the present group, and the predicted maximum width reasonably agreed with the experimental observations. Particle image velocimetry was used to measure the velocity field at the surface of the slurry layer in top and side views. A flow pattern was observed before the slurry bypassed under the roller, in the domain where variations in entrainment led to different surface profiles. Depending on the roller's rotating direction and speed, the slurry was either more effectively drawn under the roller, forming a mild ridge, or less effectively entrained, resulting in a pronounced ridge.

I. INTRODUCTION

Spreading of soft materials is an important and interesting subject that is relevant in a variety of applications, such as spreading of paper,[1] cosmetics,[2] topical medication,[3,4] food engineering,[5] as well as construction materials.[6] The substance being spread may be a single-phase or a complex multi-phase material (e.g., a mixture of solid, liquid, and/or gaseous phase). For example, in the framework of construction materials, the gypsum slurry involves materials comprised of solid particles, a foaming surfactant, and air bubbles, as well as fibers and starch, in water.

Gypsum is globally used in lightweight construction because gypsum products serve numerous functions, such as heat preservation, i.e., thermal insulation, sound absorption, and fireproofing.[7] They are manufactured by processing gypsum slurry, which is prepared by mixing gypsum stucco with water, foam, and other above-mentioned ingredients.[8] Gypsum slurries are dense cohesive granular suspensions with time-dependent rheology. Upon mixing water with calcined gypsum, the slurry initially behaves as a high-solid suspension with sufficient fluidity; yet, it ultimately undergoes hydration reactions that can significantly increase its stiffness within several minutes. The full spectrum of rheological phenomena in gypsum–water slurries exhibits non-Newtonian characteristics, including shear thinning and a notable yield stress.[9] To capture this complex rheological behavior, various constitutive models were tested, such as the Ostwald–de Waele (the power-law) model,[9] the Herschel–Bulkley model,[10] the Sisko model,[11] and the Casson model,[12] depending on the shear rate range and composition of the mix.

Spreading of soft materials may proceed on its own due to wettability or be facilitated by higher pressure domains created in the flow by applied boundary conditions. In the case of gypsum slurry, higher pressure domains can be created by spreading knives, such as hawks and trowels, applicator knives, or drawdown bars. Forming wallboard by a rotating roller over a moving belt carrying gypsum slurry (Fig. 1) also creates a high-pressure domain under the roller similar to the cases of journal bearing or screw extruders.[13–17] The relevance to industrial applications can

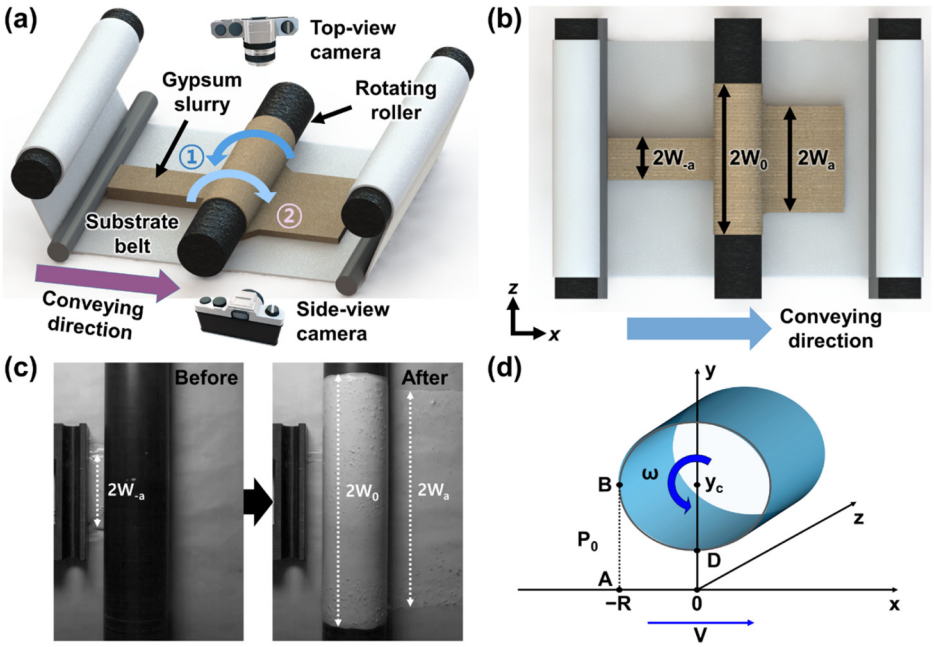

FIG. 1. Schematic of the experimental setup: (a) Isometric view and (b) top view. (c) Photographs of the gypsum slurry layer entering and exiting under the middle roller. (d) Isometric sketch of the experimental setup with the conveyor belt moving with velocity V and carrying the gypsum slurry layer into a narrow gap under a roller of radius R rotating with the angular velocity ω.

also be seen in U.S. Patent US3373065A, which describes a wallboard forming method. There, slurry is spread by a rotating roller to the desired thickness of the wallboard.

Recently, a theory of spreading under a roller in lubrication approximation was revisited to incorporate the description of the sideways spreading (i.e., spreading in the z-direction in Fig. 1).[18]

To experimentally investigate slurry flows in detail, a major obstacle is the necessity to deal with the opaque material. Optical methods, such as Particle Image Velocimetry (PIV), which track particles in fluids, are the state-of-the-art tools used to observe complex flows.[19,20] However, because conventional PIV systems typically rely on lasers as a light source, they are inadequate to be applied to non-transparent fluids, such as the gypsum slurry within a non-transparent enclosure.[21] Digital Image Correlation (DIC), on the other hand, is commonly used for analyzing deformation in opaque, solid materials, but is unsuitable for analyzing fluid flows.[22]

Several studies have attempted to overcome these challenges in opaque slurries. The x-ray imaging and Magnetic Resonance Imaging (MRI) have been employed to visualize internal flows within opaque materials.[23–25] However, x-ray imaging requires expensive equipment and is limited by spatial resolution, especially for dense particle-laden flows. Similarly, MRI provides detailed flow information but suffers from low temporal resolution and is impractical for dynamic industrial slurry flows. Ultrasonic Doppler Velocimetry (UDV) is another approach that has been used to measure velocity profiles in opaque suspensions, but it also has limited spatial resolution and is sensitive to particle concentration and acoustic properties of the medium.[26,27] These limitations hinder applicability of these methods for observing detailed flow fields in practical gypsum slurry systems.

In the present study, to address these limitations, surface observations using PIV were combined with analytical modeling. A thorough experimental study of the gypsum slurry spreading in the setup sketched in Fig. 1 is undertaken. By observing seeding particles on the slurry surface, the flow velocity was measured where optical access is possible. In the present experiments, fine and soft coffee particles were used instead of coarse tracers employed elsewhere.[28,29] It should be emphasized that Ref. 28 studied spreading of compound materials in the setting resembling spreading knife (e.g., a hawk and a trowel, an application knife, or a drawdown bar), albeit using model transparent materials (Carbopol gels). On the other hand, gypsum slurries are opaque, which is a significant complication compared to the system of Ref. 28 and are also spread using a rotating roller, which implies totally different flow kinematics. Accordingly, in the present work, only the surface flow data were acquired and then interpreted and validated using comparison with the analytical predictions. This approach allows an indirect evaluation of the internal flow characteristics of the opaque gypsum slurries. This hybrid approach also provides a practical and efficient method for studying slurry flows, overcoming the spatial and temporal resolution limitations of conventional techniques.

II. MATERIALS AND METHOD

A. Materials

The gypsum slurries used in the experiment were prepared by mixing three materials: gypsum stucco ($CaSo_4$, Sheetrock® all-purpose joint compound), a heat-resistant accelerator (a salt that promotes crystallization, HRA), and a retarder (an acid, which slows down crystallization). All the materials were provided by the United States Gypsum Corporation (USG, USA). A plastic wrap

(unbleached compostable parchment paper, Reynolds Kitchens, USA) was used as a belt conveying gypsum slurry. Note that the surface roughness of the paper used in the present study is ~8.6 μm.[30] Ground-up coffee particles (100% Colombian Coffee, Kirkland, Inc., USA) were added to gypsum slurry to serve as seeding particles in flow visualization for particle image velocimetry (PIV) measurements.

B. Preparation of gypsum slurries

For slurry with a water-stucco ratio (WSR) of 75, two mixtures were prepared separately. First, 45 g of gypsum stucco was mixed with 0.225 g of the HRA. In a separate container, 0.15 g of retarder was dissolved in 33.75 g of de-ionized water. It should be emphasized that the retarder was used to extend the working time by inhibiting slurry solidification because without adding the retarder, the slurries began to solidify on the scale of seconds after mixing. The amount of the retarder was carefully determined in the preliminary tests to ensure workability during spreading without causing an excessive delay in slurry setting. The two as-prepared mixtures were blended by a mixer (Magic bullet mini, Homeland Housewares, USA) for 10 s. Because slurries of the type described above solidify in ~1 min, the experiment was conducted right after the slurry was prepared.

C. Experimental setup

The experimental setup used to observe the flow and spreading of gypsum slurry incorporated three rollers, as shown in Fig. 1(a). Two rollers at the ends carried the paper belt at a constant speed of 0.26 m/s working as a roll-to-roll machine. The intermediate (forming) roller was located in the middle and co-rotated at an angular speed of 94, 240, or 504 rpm, no-rotated, or counter-rotated at an angular speed of −94, −240, or −504 rpm. Note also that the material of the roller can, in principle, affect the spreading process, e.g., via roughness and porosity. Therefore, in the present study, Delrin (a material commonly used in practice) was selected as the roller material in order to ensure relevance of the results for industrial settings.[31] Note also that the counterclockwise rotation of the roller corresponds to co-rotation [cf. ① in Fig. 1(a)] and the clockwise rotation corresponds to counter-rotation [cf. ② in Fig. 1(a)]. The roller surface attains the linear velocities of 0.25, 0.64, and 1.35 m/s when rotating at the angular velocities of 94, 240, and 504 rpm, respectively. This roller was made of Delrin (polyoxymethylene, Dupont, USA) with a size of 5.01 cm (diameter) × 12 cm (length). The rear conveying roller and the middle-positioned roller were powered independently by two motors (DC 12 V, Greartisan, China). Note that the rotation speed of the rollers was kept constant throughout the experiment. Changes in the width of the slurry layer caused by the middle roller were recorded by a camera (iPad Pro 3rd Gen., Apple, USA) positioned above. It measured the width of the gypsum slurry before, on, and behind the roller [see Figs. 1(b) and 1(c)].

The slurry-releasing method is illustrated in Fig. 2. Gypsum slurry was poured into a slurry holder, which was made by a 3D printer. The slurry holder was open at the bottom in such a way that the slurry inside the holder could be in contact with the conveying belt and transported by it when the latter started moving.

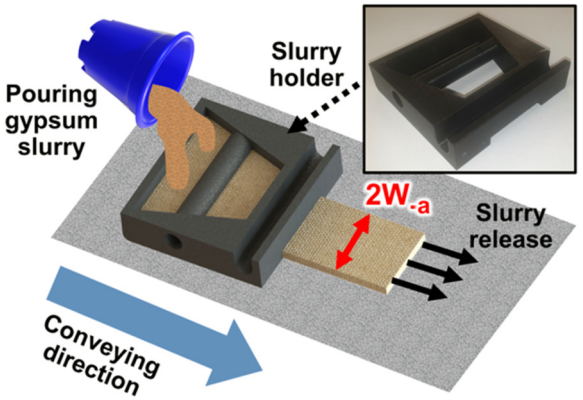

FIG. 2. Schematic of the gypsum-slurry releasing method. A photo of a slurry holder is inserted.

The slurry holder had an outlet of 5.1 cm (the width equal to $2W_{-a}$) and was 0.7 cm in height. In each experiment, slurry was supplied for approximately 3 s. The flow behavior during this period was divided into three sequential stages: (i) the development stage, where slurry built up in front of the roller; (ii) the quasi-steady stage; and (iii) the depletion stage, where the flow weakened and eventually stopped. The PIV analysis focused on the quasi-steady stage and was carried out over a time frame much shorter than the total duration of that stage. The slurry pulled by the belt from the holder maintained this width and height (due to its high viscosity) almost until it encountered the roller.

In addition, the seeding coffee particles visible at the free surface of the slurry layers were tracked by a Phantom high-speed camera (VEO-E 340L, Vision Research, USA) in the top and side views, and three repetitions were conducted in each case. The density of the coffee particles was measured to be 0.41 g/cm^3.

The particle-size distribution analysis was performed on 215 coffee particles used as PIV tracers. The size-equivalent radius ranged from 17 to 828 μm, with a mean particle size of ~90 μm (Fig. S1 in the supplementary material). The distribution exhibited a positive (right-hand side) skew, which is commonly observed in particulate systems due to fragmentation and aggregation processes.[32]

Gravity driven sedimentation of coffee particles in gypsum slurry is absolutely excluded because the density of ground coffee of $\rho_p \approx 0.4$ g/cm^3 is much less than that of gypsum slurry, which is $\rho \approx 1.6$ g/cm^3.[9]

To evaluate the potential influence of particle inertia, the particle response time to flow velocity variation (τ) was evaluated based on the Stokesian drag as

$$\tau = \frac{2\rho_p a^2}{9\mu}, \tag{1}$$

where a is the particle radius and μ is the slurry shear viscosity.

The lowest slurry viscosity at the highest shear rate is ~3 g/(cm s).[9] Accordingly, assuming the largest particle of ~1000 μm

(cf. Fig. S1 in the supplementary material) and the lowest slurry viscosity, one obtains from Eq. (1) the longest particle response time in the present experiments as $\tau \sim 10^{-4}$ s. This is of the same order as the observation timescale of the interval between PIV snapshots, which is also $\sim 10^{-4}$ s. Therefore, in the present experiments, all particles from the particle-size spectrum were fully entrained and followed the slurry flow during measurements.

Additionally, it was observed that while parts of the coffee particles dissolved in water, the process took longer than 1 min (see Fig. S2 in the supplementary material), which is a considerably longer time span than the experiment duration (~10 s). All the above estimates confirm that the effect of particle sedimentation, inertia, and dissolution on PIV measurements was negligible in the present case, which fully supports the validity of using coffee particles as tracers in the present experiments. Note that coffee particles were also successfully used as PIV tracers in another type of soft matter, specifically, in aqueous solutions of carbopol (carbopol gels) in Ref. 28.

The snapshots were analyzed with the help of two PIV software: PIVware (provided by TU Delft) for the side view and PIVlab (MATLAB source, Germany) for the top view. The use of certain software was particularly validated by ensuring that the key design parameters were met for a proper PIV analysis. Accordingly, the image density (the number of particle images per interrogation region) was maintained above 10. In addition, the interrogation region (the subareas into which an image is divided to determine a vector displacement between the corresponding images) size was adjusted to limit an in-plane displacement to less than one-fourth of the interrogation region, while an out-of-plane displacement was not a concern as the coffee particles remained on the surface. Furthermore, in PIVware, correlation averaging, which is well-suited for quasi-steady state flows such as in the present experiments, was employed to minimize noise and improve accuracy over instantaneous correlation methods.[33] On the other hand, PIVlab did not employ correlation averaging but was chosen for its ease of use. The results obtained using PIV with the background (Fig. S3 in the supplementary material) were utilized for the analysis after removing the background.

Streamlines were produced using the built-in streamlines function in MATLAB. In order to reduce noise and find streamlines only in the areas of interest, a threshold was set so that any velocities under 20 mm/s would be set to 0. This threshold eliminated producing streamlines in areas where there was no slurry and facilitated finding the characteristic streamlines of the flow.

III. RESULTS AND DISCUSSION

A. Model prediction for the case without foam

The model developed in Ref. 18 for the case of gypsum slurry involves the following six dimensionless groups:

$$\bar{a} = \frac{a}{R}, \quad \bar{y}_c = \frac{y_c}{R}, \quad \mathrm{Re} = \frac{p_0 R}{\mu V}, \quad \mathrm{Re}_\omega = \frac{p_0}{\mu\omega}, \quad \Omega = \frac{\omega R}{V}, \quad \bar{W}_{-a} = \frac{W_{-a}}{R}. \tag{2}$$

For a detailed information regarding the model, see the Appendix in the supplementary material. In particular, $x = -a$ (with a being positive) corresponds to the value of the x coordinate in Fig. 1(d) where the gypsum layer makes the first contact with the roller, i.e., essentially is associated with the initial thickness of the layer released from the device shown in Fig. 2. In addition, R is the radius of the roller [cf. Fig. 1(d)], the angular rate of the roller is denoted as ω, and the roller axis is located at $y = y_c$, and oriented in the spanwise z-direction, i.e., is parallel to the substrate belt (cf. Fig. 1). The surrounding atmospheric pressure is p_0, and the slurry viscosity is μ (assuming the slurry to be a Newtonian material in the first approximation). The belt is moving with velocity V. At $x = -a$, the half-width of the slurry layer determined by the release device of Fig. 2 is equal to W_{-a}.

The theory of Ref. 18 predicts the spanwise half-width of the gypsum slurry layer W(x) as it is spread by the roller (cf. Fig. 1) in the $-a \le x \le 0$ range. The following values of the dimensional parameters correspond to the present experiment: $a = 1.448$ cm (the initial thickness of the slurry layer was 0.651 cm), $V = 26.2$ cm/s, $R = 2.55$ cm, $y_c = 2.75$ cm, $p_0 = 1$ atm $\approx 10^6$ g/(cm s^2), $\mu = 100$ g/(cm s) according to Ref. 9, and $W_{-a} = 2.55$ cm. The corresponding values of the dimensionless groups from Eq. (2) were the following:

$$\bar{a} = 0.568, \quad \bar{y}_c = 1.078, \quad \mathrm{Re} = 973, \quad \bar{W}_{-a} = 1,$$

$$\mathrm{Re}_\omega = \begin{pmatrix} 7579 \\ 15916 \\ 40810 \\ \infty \\ -40810 \\ -15916 \\ -7579 \end{pmatrix}, \quad \Omega = \begin{pmatrix} 0.1301 \\ 0.0620 \\ 0.0242 \\ 0 \\ -0.0242 \\ -0.0620 \\ -0.1301 \end{pmatrix} \tag{3}$$

$$\text{when } \omega = \begin{pmatrix} 504 \text{ rpm} \\ 240 \text{ rpm} \\ 94 \text{ rpm} \\ 0 \text{ rpm} \\ -94 \text{ rpm} \\ -240 \text{ rpm} \\ -504 \text{ rpm} \end{pmatrix}, \text{ respectively.}$$

The theory of Ref. 18 predicts the distribution of the half-width and excess pressure $\Delta p = p - p_0$ of a slurry layer from its release location to the maximum spreading location at $x = 0$ (i.e., on the roller) as shown in Fig. 3.

The predicted half-width value corresponding to the roller [cf. the right-hand side image in Fig. 1(d)] is $\bar{W}_0 = W(0)/R \approx 2.6$ according to the result of Fig. 3(a), where W_0 is rendered dimensionless by R. The experimental values measured are 2.36, 1.84, 2.70, 2.37, 3.40, 2.26, and 3.91 for the roller rotation speeds of −504, −240, −94, 0, 94, 240, and 540 rpm, respectively. Figure 3(b) presents the excess pressure distribution Δp(x) for different values of ω. For the co-rotation and no-rotation cases, the values of Δp begin to increase from the position of $x = -0.57$, which is the location where the slurry layer encounters the roller. From that point, Δp(x) increases due to the same reason as in journal bearings, i.e., because a viscous material is entrained into a narrowing channel.

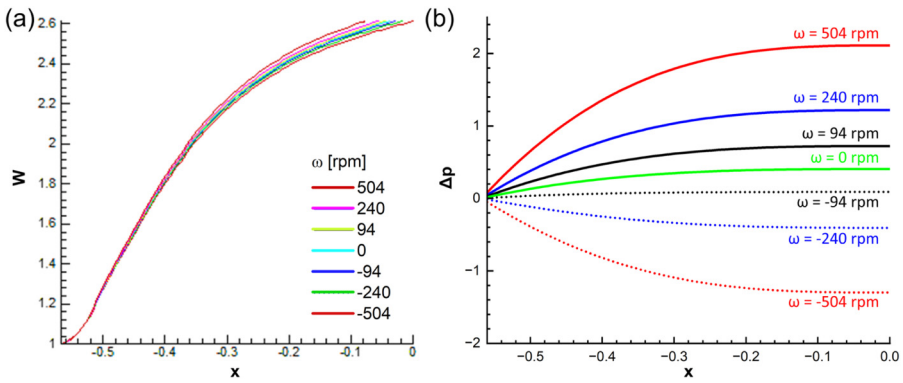

FIG. 3. Theoretical predictions. (a) Half-width W(x) predicted using Eqs. (53)–(56) from Ref. 18; curves from right to left (from red to brown) correspond to the input from Eq. (3) from top to bottom. (b) The dimensionless excess pressure $\Delta p = p - 1$ (rendered dimensionless by the atmospheric pressure p_0) in the slurry layer predicted using Eqs. (47)–(49) of Ref. 18 with the parameter values of Eq. (3). Panel (a) is predicted using Eqs. (A3.11)–(A3.17), and panel (b) is predicted using Eqs. (A3.5)–(A3.7) from the Appendix in the supplementary material.

As the entrainment by the belt is more facilitated by the entrainment by the roller (as ω increases), the pressure increase becomes more pronounced. Conversely, the values of Δp begin to decrease from the initial position when the roller counter-rotates. As the entrainment by the belt is adversely affected by the roller (as ω decreases), the pressure decrease becomes more pronounced.

Figure 4 presents the velocity component u in the x-direction predicted under the roller using the theory of Ref. 18. The velocity at $y = 0$ in all cases was the same as the substrate velocity (26.2 cm/s), and the velocity on the roller surface was determined by the roller's rotation speed. When the rotation speed ω of the roller was larger in magnitude than −94 rpm, a large reverse flow occurred ahead of the roller ($x < -0.9$ cm) [see the blue areas in Figs. 4(a)–4(e)] in concert with the corresponding pressure distributions presented in Fig. 3(b). In the co-rotation cases [Figs. 4(a)–4(c)], the flow below the roller was in the same direction as the substrate and the roller motion, strengthening at higher values of ω [cf. Figs. 4(a)–4(d)]. In the case of the middle and high magnitude counter-rotation in Figs. 4(f) and 4(g), the counter-flow ahead of the roller diminished and shrank toward the roller, in concert with the corresponding pressure distributions presented in Fig. 3(b), whereas under the roller, almost the entire material was entrained backward by the roller as the rate of counter-rotation enhanced.

Figure 5 presents the fields of the predicted y-velocity v in the roller co-rotation, no-rotation, and counter-rotation cases corresponding to those in Fig. 4. The negative values of v near the substrate in the co-rotation cases in Figs. 5(a)–5(c) stem from the tendency to develop a reverse flow discussed in relation to Fig. 4. In the non-rotation case in Fig. 5(d), there is no vertical flow under the roller. In the counter-rotation cases in Figs. 5(e)–5(g), the positive values of v stem from the entrainment by the roller.

B. Experimental results

1. Measured half-widths of slurry layers

Figure 6 presents the measured width ratios of the slurry layers at different roller rotation speeds corresponding to co-rotation (positive rpm), no-rotation (0 rpm), and counter-rotation (negative rpm). The lowest rotation speed was also the highest-in-magnitude counter-rotation speed (cf. −504 rpm). The experimentally observed width ratio varied between 1.5 and 4.0, while the theoretical value being ∼2.6 [see Fig. 3(a)]. Although slight deviations are observed at the roller rotational speeds of −240, 0, and 240 rpm, these cases still reveal the width proportionality to the roller speed. This overall trend can be attributed to an enhanced squeezing effect as the rotational speed increases. Specifically, higher rotational speeds cause stronger squeezing forces, leading to an increased pressure in the slurry [cf. the theoretical predictions in Fig. 3(b)]. This promotes lateral spreading toward the edges where no physical constraints impede the flow. Additionally, an increased rotational speed enhances shear-thinning tendencies in the rheological behavior of the slurry, which facilitates flowability.[34] As a result, the width ratio increases with the roller rotational speed. The width recovery after the slurry passes through the roller, as indicated by the W_a/W_{-a} value (the red line in Fig. 6), was consistently smaller than the value of W_0/W_{-a} (the black line in Fig. 6), which means that the slurry layer contracts after leaving the roller because the substrate (the parchment paper) is non-wettable (see Fig. 7).

Figure 7 illustrates the wettability of the substrate paper by water and slurry (cf. Sec. II A). 0.2 ml of water or slurry was put on a plastic (parchment paper) and observed for 20 min. The water drop is formed an angle close to 90°, which stayed practically unchanged, revealing that water did not wet the plastic, and the plastic surface can be characterized as hydrophobic [Fig. 7(a)]. The initially higher apparent contact angle of the gypsum slurry (94°) compared to that of water (92°), as in Fig. 7(b), may suggest enhanced hydrophobicity. However, this is a transient phenomenon. Later on, gypsum hydration and water evaporation cause a reduction in the droplet volume, resulting in a decreased apparent contact angle.

2. Side view of the flow field of slurry near the roller

Particle image velocimetry (PIV) was employed to observe and characterize the flow fields in the slurry layers entrained under

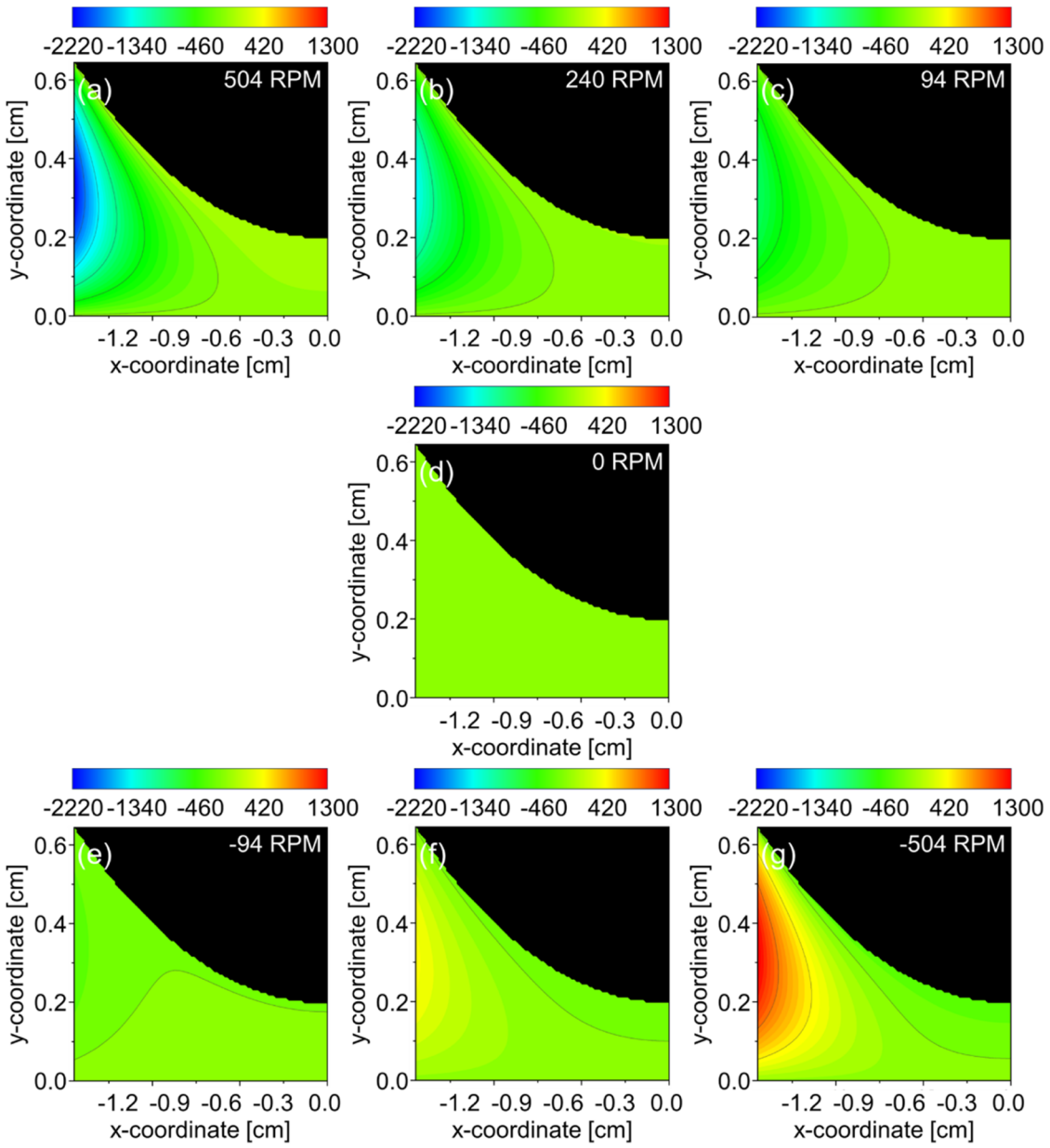

FIG. 4. Theoretically predicted x-velocity component u in the side view of gypsum slurry entrained under a roller. The parameter values of Eq. (3) were used. Rotation speed: (a) 504, (b) 240, (c) 94, (d) 0, (e) −94, (f) −240, and (g) −504 rpm. The color bar corresponds to the values of u in cm/s. Predicted using Eqs. (A1.10) and (A3.5)–(A3.7) in the supplementary material.

the roller, as shown in Figs. 8–10. To the best of our knowledge, PIV applications aiming for measurements of velocity fields in opaque media are scarce.[21,35,36] The present approach employing PIV based on particles deposited at the free surface of gypsum slurry is a new example of this kind. In all cases, the upper part of the slurry layer moved at a low speed of less than 0.002 m/s before meeting with the roller, whereas the lower part close to the belt moved at a relatively high speed of 0.200–0.254 m/s as the main cause of movement is the conveyor belt (see Fig. S4 in the supplementary material).

In the co-rotation case illustrated in Fig. 8 (Multimedia available online), the entire slurry layer was entrained under the roller and

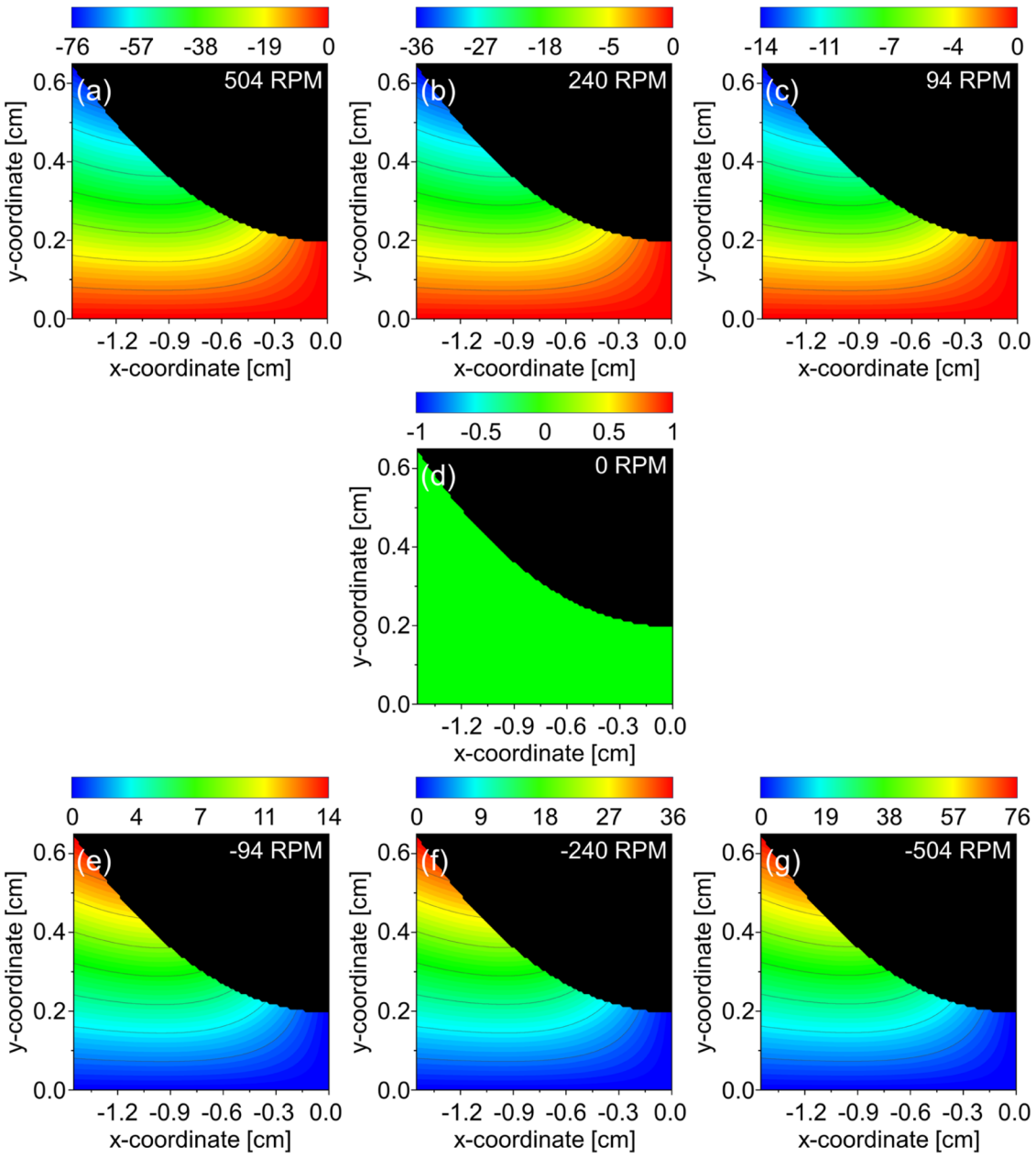

FIG. 5. Theoretically predicted y-velocity component v in the side view of gypsum slurry entrained under a roller. The parameter values of Eq. (3) were used. Rotation speed: (a) 504, (b) 240, (c) 94, (d) 0, (e) −94, (f) −240, and (g) −504 rpm. The color bar corresponds to the values of v in cm/s. Predicted using Eqs. (A1.11) and (A3.5)–(A3.7) in the supplementary material.

flowed through the gap between the substrate and the roller. The upper part of the slurry layer moved slower than the lower part of the layer. The reason is the following: the upper part was mostly entrained by the co-rotating roller. This part of the flow was already affected by the adverse pressure gradient building up in the narrowing gap, whereas the lower part of the slurry layer was entrained by the moving belt (which had a velocity of 0.262 m/s). In Fig. 8 (Multimedia available online), the slurry thicknesses at the leftmost position, measured in the direction perpendicular to the belt, were 3.8, 3.0, and 3.5 mm for roller speeds of 94, 240, and 540 rpm, respectively.

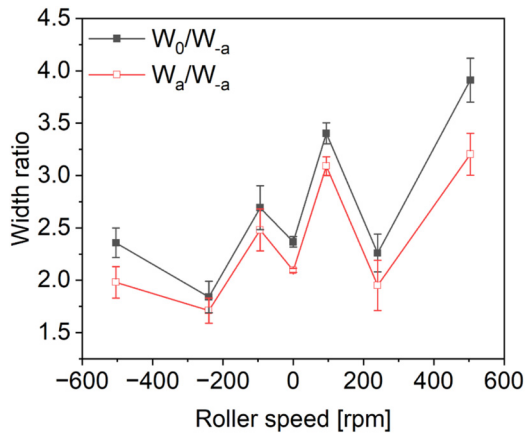

FIG. 6. Overall width ratios of gypsum slurry layers as functions of the rotational speed of the roller.

Near the roller, its rotational speed significantly affected the slurry flow. As in the case of a low-speed rotation [see Fig. 8(a)], the slurry flow formed a hill-like zone behind the roller as a result of significant previous squeezing under the roller. The slurry velocity in this zone was relatively low (<0.004 m/s). The zone exhibited varying characteristics depending on the roller rotation. The maximum thicknesses of this zone were 6.5 and 7.1 mm for 94 and 240 rpm, respectively. For 540 rpm, it was difficult to identify the hill-like zone.

Velocity components u in the x-directions, corresponding to the flow fields of Fig. 8 (Multimedia available online), are presented in Fig. S5 of the supplementary material. It reveals no discernible reverse flow in almost all the cases of a co-rotating roller. Although over-entrainment resulted in the reverse flow, as in Figs. 4(a)–4(c), its extent was localized, and it appeared in the other (spanwise) direction, as shown in Fig. 6, with an increase in the width ratio larger than the theoretical value of ∼2.6.

At a low rotation speed of the roller [as in Fig. S5(a) of the supplementary material], the forward flow velocity near the conveyor belt increases when the flow approaches the roller. As the roller speed is increased to 504 rpm [as in Fig. S5(c) of the supplementary material], the velocity component u is observed to significantly increase, which corresponds to the forward flow results depicted in Fig. 4. Given that the corresponding pressure is higher than that in the lower speed co-rotation case (see Fig. 3), the higher speed of the co-rotating roller facilitates the conveyance of the slurry at a faster rate in the direction of both the conveyor belt and in the width direction, resulting in a higher width ratio as in Fig. 6.

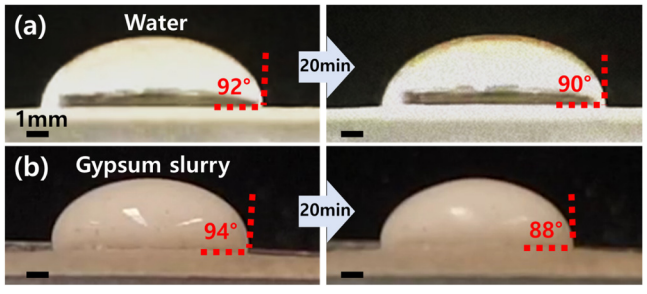

FIG. 7. Changes in the apparent contact angle in 20 min of (a) water and (b) gypsum slurry.

In the exceptional case of 240 rpm [Fig. S5(b) in the supplementary material], the forward flow before the roller increases significantly; yet, the flow under the roller is suppressed. Theoretically, this middle speed co-rotating roller should have resulted in a moderate pressure level [Fig. 3(b)] and a moderate-range velocity (Fig. 4), but instead, it exhibits an exceptional flow with the lowest width ratio (Fig. 6).

In the co-rotation case with a low roller speed [Figs. S6(a)–S6(c) in the supplementary material], which corresponds to the results in Figs. 8(a)–8(c), negative velocity components v were observed in the domain where the x-direction velocity is significant (see Fig. S5 in the supplementary material), which may be attributed to the effect of the roller. The range and magnitude of these velocities were found to be small ($-v < 0.1$ m/s) in comparison with the rotation speed of the roller. As the rotation speed of the roller increased from 94 to 504 rpm [Figs. S6(a) and S6(c) in the supplementary material], the downward velocity domain exhibited a notable enlargement. In the exceptional case of 240 rpm [Fig. S6(b) in the supplementary material], the downward flow was comparatively weaker than in the other cases, with its maximum magnitude occurring before the roller and subsequently diminishing in its vicinity.

In the case of the non-rotating roller (see Fig. 9, Multimedia available online), the slurry layer was completely entrained under the roller as in the co-rotation cases with moderate rotation speeds of the roller [Fig. 8(b)].

In Fig. 9 (Multimedia available online), the slurry flow formed a hill-like stagnation zone behind the roller, similar to the co-rotation case, here with the maximum thickness of 7.1 mm.

The field of the velocity component u (Fig. S7 in the supplementary material) was similar to the co-rotation cases with a moderate rotation speed [Fig. S5(b) in the supplementary material]. In the absence of rotational movement, the flow domain was observed to be broader than that observed in the moderate co-rotation case [see Fig. S5(b) in the supplementary material]. This phenomenon may be attributed to the formation of low adverse pressure under the roller, as illustrated in Fig. 3(b), which, in turn, gives rise to a larger width ratio (Fig. 6). However, it is noteworthy that the flow domain in the non-rotating roller case was significantly different from that observed in the co-rotation cases with rotation speeds of 94 and 504 rpm [Figs. S5(a) and S5(c) in the supplementary material], which resulted in a distinct trend in the width ratio (Fig. 6).

In the case without roller rotation (see Fig. S8 in the supplementary material), negative velocity components v were observed in the domain where the x-direction velocity was significant (Fig. S7 in the supplementary material), as was the case in the co-rotation cases (cf. Figs. S5 and S6 in the supplementary material).

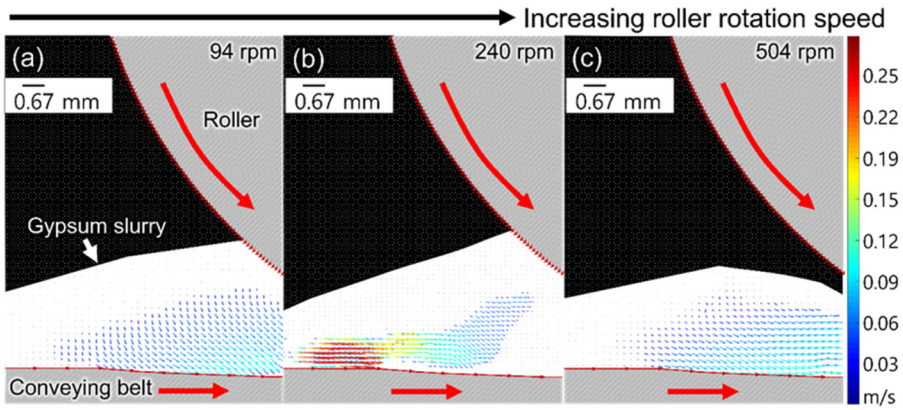

FIG. 8. Vector flow field (the side view) of gypsum slurry entering under a co-rotating roller. Rotation speed: (a) 94, (b) 240, and (c) 504 rpm. The color bar characterizes the velocity magnitude. Multimedia available online.

In the absence of rotational motion, the flow domain was observed to be broader than that observed in the moderate co-rotation case [Fig. S6(b) in the supplementary material]. This is opposite to the theoretical expectations (Fig. 5). It may imply that a stronger downward flow is related to a higher width ratio than that in the 240 rpm case in Fig. 6.

In the case of the counter-rotation roller illustrated in Fig. 10 (Multimedia available online), the slow-motion zone behind the roller was significantly decreased due to the roller turning in the opposite direction to that of the belt. This resulted in a stronger rejection of the slurry on the entry side of the roller. Instead, only a portion of the slurry layer was entrained under the roller, while the rest was removed along the roller.

Figure 10 and Fig. S4 in the supplementary material reveal that the upper part of the slurry layers moves slower than the lower part before being entrained under the roller. Additionally, at $\omega = -94$ rpm, the leftmost section of the slurry layer possessed a thickness of 3.7 mm, while for the rotation speeds of −240 and −504 rpm, the thicknesses were 3.3 mm and 2.4 mm, respectively. A decrease in the roller speed resulted in a decrease in the slurry supply width.

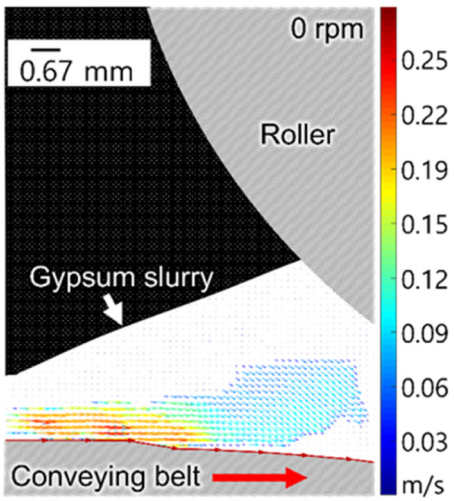

FIG. 9. Vector flow field (the side view) of gypsum slurry entrained under a no-rotating roller. The color bar characterizes the velocity magnitude. Multimedia available online.

The rotation speed of the roller had a significant impact on the slurry motion. When the roller rotated at a low speed [cf. Fig. 10(a)], the slurry was carried along with the counter-rotating roller, resulting in a maximum height of 11.2 mm. At $\omega = -240$ rpm, a slurry layer was formed on the roller and carried by it, as it rotated. The height increased to 19.2 mm. At $\omega = -504$ rpm, a layer was formed on the roller but not carried away by it because the rotational speed was too fast. The height was larger than for the low speed but less than for the moderate speed: 14.3 mm.

Figure S9 in the supplementary material illustrates the field of the velocity component u in the counter-rotation case, where the adverse-pressure-caused reverse flow was difficult to detect. Although some signs of the reverse flow can be seen near the roller, they were caused by the entrainment of slurry by the roller [as seen in the red patches of Figs. S9(a) and S9(b) in the supplementary material]. The extension and magnitude of the reverse flow are minimal in Fig. S9 of the supplementary material, making it challenging to determine any correlation with the roller speed.

Similarly to the moderate co-rotation case [Fig. S5(b) in the supplementary material], in the counter-rotation case, at a low roller rotation speed [Fig. S9(a) in the supplementary material], the forward (in the x-direction) flow becomes weaker in the vicinity of the roller. The effect of the roller speed was evident at the counter-rotation speed of 240 rpm, which enabled a faster slurry transport in the x-direction [Fig. S9(b) in the supplementary material], corroborating the outcome depicted in Figs. 3(b) and 4. However, as the roller speed increased further (504 rpm), the x-direction flow exhibited slight suppression [Fig. S9(c) in the supplementary material].

In the case of counter-rotation [cf. Figs. S10(a) and S10(b) in the supplementary material], strong red patches ($|v| < 0.1$ m/s) were observed in the vicinity of the roller, possibly due to the slurry entrainment by the roller. However, only a limited number

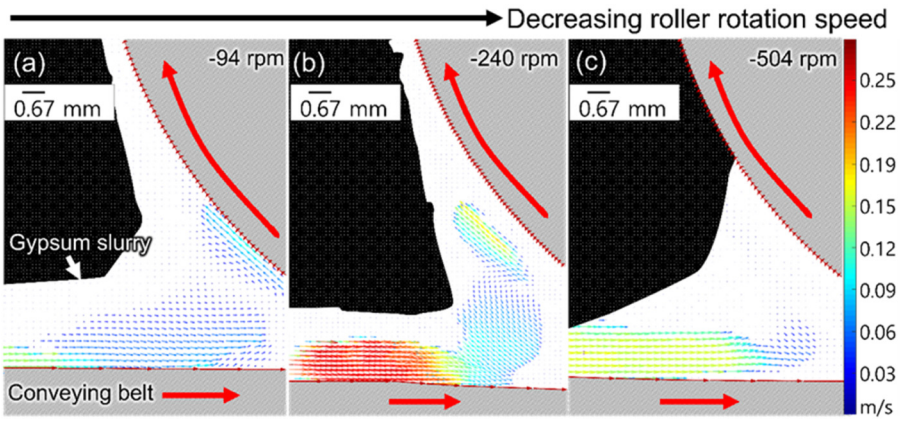

FIG. 10. Vector flow field (the side view) of gypsum slurry entrained under a counter-rotating roller. The rotation speed: (a) −94, (b) −240, and (c) −504 rpm. The color bar characterizes the velocity magnitude. Multimedia available online.

of domains exhibited a pronounced upward flow. As the roller rotation speed was varied from −94 to −240 rpm [Figs. S10(a) and S10(b) in the supplementary material], the vertical flow enhanced, as indicated by the range of the color bar. At a high roller rotation speed [Fig. S10(c) in the supplementary material], the vertical motion of the slurry practically disappeared. However, it should be emphasized that in the fastest counter-rotation case, a rough slurry layer was observed on the roller surface; it even spilled outward.

The theoretical results regarding the flow field depicted in Figs. 4 and 5 are, essentially, accurate not in the entire gap below the roller, but rather at the narrowest part of it, due to the simplifications embedded in the theory of Ref. 18. Accordingly, the theory was rather accurate in predicting the widening of the slurry layer on the roller, as discussed above. On the other hand, the predicted flow field around the narrowest cross section under the roller should be considered only as a qualitative guidance complimenting the experimental patchy data provided by the PIV, where the x range of [−1.4 cm, 0 cm] was explored rather than $x \approx 0$. The theory predicts a significant reverse flow near the entrance to the roller at $\omega > -94$ rpm (Fig. 4), whereas almost no reverse flow was observed via the PIV results (Figs. S5 and S7 in the supplementary material). Similarly, in the cases with $\omega < -94$ rpm, the PIV results [Figs. S9(b) and S9(c) in the supplementary material] revealed that, in distinction from the theoretical prediction (Fig. 5), no strong forward flow was observed. In the y-direction, the downward flow was observed in the co- and non-rotating cases (Figs. S6 and S8 in the supplementary material), but this tendency was not proportional to the speed of the roller, as expected theoretically. Similarly, the upward flow was partially observed in the counter-rotating case (Fig. S10 in the supplementary material), but it was also not proportional to the roller speed, as expected theoretically. In addition to the inevitable theoretical simplifications, discussed above, there may be one more reason for the discrepancies. The observations by PIV were limited to the slurry surface, whereas the above-mentioned theoretical results in Figs. 4 and 5 correspond to the median cross section of the slurry layer.

3. Streamlines of the slurry flow near the roller

Figure 11 illustrates the streamlines of the slurry flow in the cases of co-rotation (240 rpm), no-rotation (0 rpm), and counter-rotation (−240 rpm). In all cases, a stagnation zone is observed at the top layer of the slurry before the roller, as illustrated in Figs. 8(b)–10(b), where no streamlines are found. From the stagnation zone, some spurious streamlines could be generated, necessitating consideration of the three-dimensional nature of the flow.

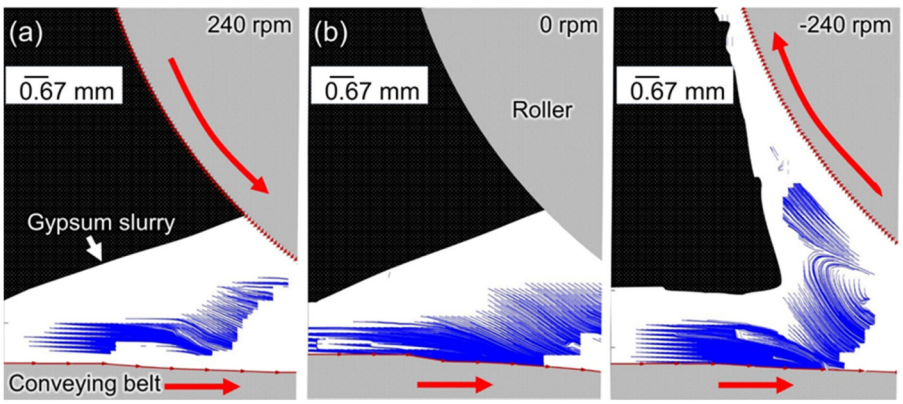

FIG. 11. Streamlines from the sideview for the (a) co-rotation (240 rpm), (b) no-rotation, and counter-rotation (−240 rpm) cases.

The streamline with the co-rotating roller [Fig. 11(a)] exhibits the shortest recognizable streamlines of the three cases, indicating that the flow is more complex in three dimensions. In the absence of rotation [Fig. 11(b)], the streamlines converge under the roller, which is consistent with the theoretical predictions. In the case of counter-rotation [Fig. 11(c)], once the slurry is entrained under the roller, a significant degree of rejection is observed, resulting in the top layer of the slurry being carried by the roller in a counterclockwise direction. Beneath this layer, the slurry is rejected and subsequently moves downward toward the substrate.

4. Lateral flow of gypsum slurry pulled under the roller recorded in the top view

Figure 12 (Multimedia available online) presents the distribution of the lateral velocity component w of gypsum slurry entrained under the roller. These observations were done from above, as sketched in Fig. 12(a). Note that the longer vectors visible on the left- and right-hand sides of the panels correspond to the measured velocity of the bottom substrate, i.e., predominantly to the velocity component u. The lateral velocity component w is characterized by color. Overall, the positive and negative values of w attest to a significant lateral flow of the impingement type, which is more or less symmetrically deflected to the left or right resulting from the pressure generated by the roller. Moreover, the comparison of Figs. S5–S10 in the supplementary material reveals that the magnitudes of the velocity components u, v, and w are of the same order, which means that the lateral flow arising when a layer of gypsum slurry is entrained under the roller is significant and, thus, is responsible for significant widening of the layer, i.e., for the dependence $W = W(x)$ of the type of the ones characterized by Figs. 3 and 6. The average spreading velocity component w decreased was 0.12 m/s.

Figure 12(b) characterizes the lateral spreading in the no-rotation cases. It attests that the highest value of the lateral velocity component w achieved was ∼0.15 m/s. The overall flow structure was similar to the co-rotation case with a moderate roller speed [Fig. 12(d)], which means that a roller with an adequate rotation speed facilitated the slurry transport without widening the slurry layer.

Figures 12(f)–12(h) present the PIV results for the counter-rotation case. The maximum velocity component w achieved (∼0.10 m/s) is approximately the same as the average value of w in the co-rotation case [Fig. 12(c)]. These values are inconsistent with the results in Fig. 6, where the layer width increase was much higher for the co-rotation case than for the counter-rotation case. Note that the results for the lateral velocity component w discussed here cannot fully characterize the lateral spreading up to the half-width W_0 of Fig. 6, because here, only the layer part visible outside the roller is considered [cf. Fig. 12(a)]. Overall, the slurry spreading velocity component w in the counter-rotating cases was similar regardless of the roller rotation speed: at a low rotation speed of 94 rpm, $w < 0.13$ m/s, at a moderate rotation speed of −240 rpm, $w < 0.09$ m/s, and at a high rotation speed of −504 rpm, $w < 0.09$ m/s. However, considering the maximum value of u in

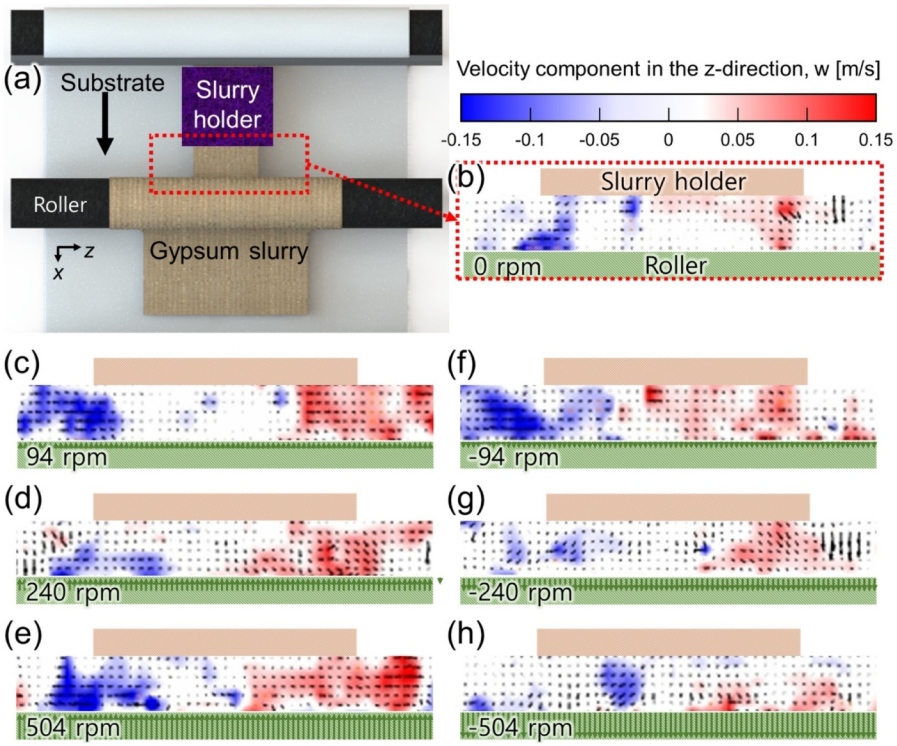

FIG. 12. (a) Schematic of the observation area. Flow field and the lateral velocity component w of gypsum slurry entrained under the roller recorded in the top view. Rotation speed: (b) 0 rpm, (c) 94 rpm, (d) 240 rpm, (e) 504 rpm, (f) −94 rpm, (g) −240 rpm, and (h) −504 rpm. Arrows correspond to the velocity vectors. The color bar represents the velocity component in the z-direction, w. Multimedia available online.

each case in Fig. S5 of the supplementary material, the moderate rotation-speed case revealed the best longitudinal transport in the x-direction, with a thinner slurry thickness.

IV. CONCLUSION

The primary objective of the present study is to quantitatively analyze spreading of gypsum slurry depending on the roller's rotational speed. Owing to the inherent challenges associated with the observation of the internal flow in opaque gypsum slurry, surface flow observations were conducted utilizing coffee particles in conjunction with particle image velocimetry (PIV). Given the fact that this method is only capable of capturing surface flow and does not directly reflect the entire three-dimensional bulk flow, a hybrid approach combined with analytical modeling was adopted. Such a hybrid approach elucidates the internal flow structure, as well as its predictions are in good agreement with the measured spreading width. Experiments with a spreading slurry gypsum layer (at the water-to-stucco ratio, WSR 75, without foam) on a moving plastic belt made of parchment paper were conducted using fine coffee particles as tracers to enable the surface flow measurements. The roller in the middle was either at rest (non-rotating), or co-rotating and counter-rotating compared to the direction motion of the plastic belt. It was shown that the belt was non-wettable by water and slurry without foam.

In general, an increase in the width of the deposited slurry layer was observed as the rotation of the roller was in the flow direction (co-rotation) and as its forward rotation speed increased. The ratio of the slurry-layer width to the original layer width was measured as 2.36, 1.84, 2.70, 2.37, 3.40, 2.26, and 3.91 for the roller rotation speed of −504, −240, −94, 0, 94, 240, and 540 rpm, respectively. The theoretical predictions reveal that the ratio would exhibit an upward trend in conjunction with an increase in the roller speed, ultimately attaining a value of ∼2.6. However, the theoretical predictions are limited by the assumption of the Newtonian rheological behavior of slurry and does not account for the potential presence of foam in the slurry. Consequently, generalization of the theory in future will facilitate research toward an optimal roller speed for on-demand efficient spreading under such given conditions as the conveyor belt speed and the geometric sizes restricting the flow.

The findings of this study offer valuable insights for the industries where a precise on-demand control of soft material spreading is crucial. Specifically, the developed measurement method can be applied to optimize coating processes in such fields as battery manufacturing, printed electronics, biomedical devices, and construction materials involving gypsum-based slurries. By providing quantitative data on spreading dynamics, the present results potentially lead to better process control, reducing material waste and improving product quality.

SUPPLEMENTARY MATERIAL

See the supplementary material for (i) details of the coffee particles used for particle image velocimetry (PIV), (ii) the original unprocessed images prior to PIV filtering, (iii) detailed PIV results, and (iv) a comprehensive explanation of the theoretical model applied in this study.

ACKNOWLEDGMENTS

The authors are grateful for the support provided by the United States Gypsum.

AUTHOR DECLARATIONS

Conflict of Interest

The authors have no conflicts to disclose.

Author Contributions

Y.K. and C.S. contributed equally to this work.

Yong Il Kim: Conceptualization (equal); Formal analysis (equal); Investigation (equal); Methodology (equal); Validation (equal); Visualization (equal); Writing – original draft (equal). **Caesar Sanchez:** Data curation (lead); Methodology (lead); Validation (supporting); Visualization (equal); Writing – original draft (equal). **David Podstawski:** Data curation (lead); Formal analysis (equal); Methodology (equal); Software (lead); Validation (supporting); Visualization (supporting); Writing – original draft (supporting). **Jerry Westerweel:** Software (lead); Validation (equal); Writing – review & editing (equal). **Alexander L Yarin:** Conceptualization (equal); Funding acquisition (equal); Project administration (equal); Resources (equal); Supervision (equal); Validation (equal); Writing – review & editing (equal).

DATA AVAILABILITY

The data that support the findings of this study are available from the corresponding author upon reasonable request.

REFERENCES

[1]I. Brazinsky, H. Cosway, C. Valle, Jr., R. C. Jones, and V. Story, "A theoretical study of liquid-film spread heights in the calendering of Newtonian and power law fluids," J. Appl. Polym. Sci. **14**, 2771–2784 (1970).
[2]K. Kusakari, M. Yoshida, F. Matsuzaki, T. Yanaki, H. Fukui, and M. Date, "Evaluation of post-application rheological changes in cosmetics using a novel measuring device: Relationship to sensory evaluation," J. Cosmet. Sci. **54**, 321–333 (2003).
[3]U. Ivens, B. Steinkjer, J. Serup, and V. Tetens, "Ointment is evenly spread on the skin, in contrast to creams and solutions," Br. J. Dermatol. **145**, 264–267 (2001).
[4]M. Loeffel, S. J. Ferguson, L.-P. Nolte, and J. H. Kowal, "Vertebroplasty: Experimental characterization of polymethylmethacrylate bone cement spreading as a function of viscosity, bone porosity, and flow rate," Spine **33**, 1352–1359 (2008).
[5]M. Bourne, *Food Texture and Viscosity: Concept and Measurement* (Elsevier, Amsterdam, 2002).
[6]J. S. Raucci, R. T. Cecel, R. C. d. O. Romano, R. G. Pileggi, and V. M. John, "Effect of mixing method on the mini-slump spread of Portland cement pastes," Rev. IBRACON Estrut. Mater. **11**, 410–431 (2018).
[7]Y. Li and S. Ren, *Building Decorative Materials* (Elsevier, Amsterdam, 2011).
[8]D. Dannessa, S. Sinha-Ray, S. Jun, and A. L. Yarin, "Jets of three-phase power-law fluids and foam jet mixing in gypsum slurry," Constr. Build. Mater. **166**, 922–944 (2018).
[9]S. Sinha-Ray, R. Srikar, C. C. Lee, A. Li, and A. L. Yarin, "Shear and elongational rheology of gypsum slurries," Appl. Rheol. **21**, 63071 (2011).
[10]C. Liu, J. Gao, Y. Tang, and X. Chen, "Preparation and characterization of gypsum-based materials used for 3D robocasting," J. Mater. Sci. **53**, 16415–16422 (2018).

[11]R. M. Turian, T. W. Ma, F. L. G. Hsu, and D. J. Sung, "Characterization, settling, and rheology of concentrated fine particulate mineral slurries," Powder Technol. **93**, 219–233 (1997).
[12]M. Sadeghi, S. G. Sontti, E. Zheng, and X. Zhang, "Computational fluid dynamics (CFD) simulation of three–phase non–Newtonian slurry flows in industrial horizontal pipelines," Chem. Eng. Sci. **270**, 118513 (2023).
[13]H. Schlichting, *Boundary Layer Theory* (Springer, Heidelberg, 1961).
[14]J. A. Tichy, "Hydrodynamic lubrication theory for the Bingham plastic flow model," J. Rheol. **35**, 477–496 (1991).
[15]S. J. Weinstein and K. J. Ruschak, "Coating flows," Annu. Rev. Fluid Mech. **36**, 29–53 (2004).
[16]Z. Tadmor and C. G. Gogos, *Principles of Polymer Processing* (John Wiley & Sons, New York, 2006).
[17]L. G. Loitsyanskii, *Mechanics of Liquids and Gases* (Elsevier, Amsterdam, 2014).
[18]J. Plog and A. L. Yarin, "Speed of sound in gypsum slurries with foaming agent and expected spanwise spreading," Exp. Fluids **64**, 125 (2023).
[19]R. Adrian and J. Westerweel, *Particle Image Velocimetry* (Cambridge University Press, New York, 2011).
[20]C. Poelma, "Measurement in opaque flows: A review of measurement techniques for dispersed multiphase flows," Acta Mech. **231**, 2089–2111 (2020).
[21]B. Xu, S. Zhou, F. He, F. Wang, and J. Guo, "Using particle image velocimetry to evaluate the displacement efficiency of drilling mud in horizontal well cementing," J. Pet. Sci. Eng. **195**, 107647 (2020).
[22]P. Zhang, S. D. Peterson, and M. Porfiri, "Combined particle image velocimetry/digital image correlation for load estimation," Exp. Therm. Fluid Sci. **100**, 207–221 (2019).
[23]S. J. Lee and S. Kim, "Simultaneous measurement of size and velocity of microbubbles moving in an opaque tube using an x-ray particle tracking velocimetry technique," Exp. Fluids **39**, 492–497 (2005).
[24]S. J. Lee and G. B. Kim, "X-ray particle image velocimetry for measuring quantitative flow information inside opaque objects," J. Appl. Phys. **94**(5), 3620–3623 (2003).
[25]S. Discetti and F. Coletti, "Volumetric velocimetry for fluid flows," Meas. Sci. Technol. **29**, 042001 (2018).
[26]T. L. Szabo and L. Thomas, *Diagnostic Ultrasound Imaging: Inside Out* (Academic Press, 2013).
[27]F. Ein-Mozaffari, C. P. J. Bennington, G. A. Dumont, and D. Buckingham, "Measuring flow velocity in pulp suspension mixing using ultrasonic Doppler velocimetry," Chem. Eng. Res. Des. **85**, 591–597 (2007).
[28]D. D. Pelot, N. Klep, and A. L. Yarin, "Spreading of carbopol gels," Rheol. Acta **55**, 279–291 (2016).
[29]H. D. Le, E. H. Kadri, S. Aggoun, J. Vierendeels, and P. Troch, "Effect of lubrication layer on velocity profile of concrete in a pumping pipe," Mater. Struct. **48**, 3991–4003 (2015).
[30]D. Maddipatla, B. B. Narakathu, M. Ochoa, R. Rahimi, J. Zhou, C. K. Yoon, H. Jiang, H. Al-Zubaidi, S. O. Obare, M. A. Zieger, and B. Ziaie, "Rapid prototyping of a novel and flexible paper based oxygen sensing patch via additive inkjet printing process," RSC Adv. **9**, 22695–22704 (2019).
[31]L. Tokarz, S. Pawlowski, and M. Kedzierski, "Polyoxymethylene applications," in *Polyoxymethylene Handbook: Structure, Properties, Applications and Their Nanocomposites* (Scriverner Publishing, 2014), pp. 153–161.
[32]V. A. Snyder and M. A Vázquez, "Similarities in evolution of aggregate size distributions during successive wetting and drying cycles of heavy textured soils of variable clay mineralogy," Hydrology **9**, 30 (2022).
[33]C. D. Meinhart, S. T. Wereley, and J. G. Santiago, "A PIV algorithm for estimating time-averaged velocity fields," J. Fluids Eng. **122**, 285–289 (2000).
[34]D. D. Pelot, R. P. Sahu, S. Sinha-Ray, and A. L. Yarin, "Strong squeeze flows of yield-stress fluids: The effect of normal deviatoric stresses," J. Rheol. **57**, 719–742 (2013).
[35]G. K. Auernhammer, S. Fataei, M. A. Haustein, H. P. Patel, R. Schwarze, E. Secrieru, and V. Mechtcherine, "Transparent model concrete with tunable rheology for investigating flow and particle-migration during transport in pipes," Mater. Des. **193**, 108673 (2020).
[36]H. Zheng, L. Liu, L. Williams, J. R. Hertzberg, C. Lanning, and R. Shandas, "Real time multicomponent echo particle image velocimetry technique for opaque flow imaging," Appl. Phys. Lett. **88**, 261915 (2006).